Wind-Friendly Flexible Ramping Product Design in Multi-Timescale Power System Operations

Mingjian Cui, *Member, IEEE*, Jie Zhang, *Senior Member, IEEE*, Hongyu Wu, *Senior Member, IEEE*, and Bri-Mathias Hodge, *Member, IEEE*

***Abstract*—With increasing wind power penetration in the electricity grid, system operators are recognizing the need for additional flexibility, and some are implementing new ramping products as a type of ancillary service. However, wind is generally thought of as causing the need for ramping services, not as being a potential source for the service. In this paper, a multi-timescale unit commitment and economic dispatch model is developed to consider the wind power ramping product (WPRP). An optimized swinging door algorithm with dynamic programming is applied to identify and forecast wind power ramps (WPRs). Designed as positive characteristics of WPRs, the WPRP is then integrated into the multi-timescale dispatch model that considers new objective functions, ramping capacity limits, active power limits, and flexible ramping requirements. Numerical simulations on the modified IEEE 118-bus system show the potential effectiveness of WPRP in increasing the economic efficiency of power system operations with high levels of wind power penetration. It is found that WPRP not only reduces the production cost by using less ramping reserves scheduled by conventional generators, but also possibly enhances the reliability of power system operations. Moreover, wind power forecasts play an important role in providing high-quality WPRP service.**

***Index Terms*—Dynamic programming, economic dispatch, ramping reserve, swinging door algorithm, unit commitment, wind power ramping product.**

NOMENCLATURE

A. Acronyms (Alphabetically)

AACEE	Absolute area control error in energy.
ACE	Area control error.
AGC	Automatic generation control.
CAISO	California Independent System Operator.
CPS2	Control Performance Standard 2.
DU	Day-ahead unit commitment model.
FESTIV	Flexible Energy Scheduling Tool for Integration of Variable Generation.
ISO	Independent system operator.
NERC	North American Electric Reliability Corporation.
OpSDA	Optimized swinging door algorithm.
PJM	Pennsylvania-New Jersey-Maryland Interconnection.
RU	Real-time unit commitment model.
RE	Real-time economic dispatch model.
WPR	Wind power ramp.
WPRP	Wind power ramping product.

B. Sets and Parameters

b	Index for buses, $b = 1, 2, ..., NB$.
$e_{(\cdot)}$	End time of a WPRP.
$\overline{e_{(\cdot)}}$	End time of a non-WPRP.
i	Index for thermal units, $i = 1, 2, ..., NI$.
m	Index of the mth WPRP.
p_u^w	Wind power value at time period u.
$s_{(\cdot)}$	Start time of a WPRP.
$\overline{s_{(\cdot)}}$	Start time of a non-WPRP.
$t^{(\cdot)}$	Index for time periods. $t^{\mathrm{DU}} = 1, 2, ..., T^{\mathrm{DU}}$ in DU model; $t^{\mathrm{RU}} = 1, 2, ..., T^{\mathrm{RU}}$ in RU model, $t^{\mathrm{RU}} \in t^{\mathrm{DU}}$; and $t^{\mathrm{RE}} = 1, 2, ..., T^{\mathrm{RE}}$ in RE model, $t^{\mathrm{RE}} \in t^{\mathrm{RU}}$.
$\triangle t^{(\cdot)}$	Time resolution in minute. $\triangle t^{\mathrm{DU}} = 60$, $\triangle t^{\mathrm{RU}} = 15$, and $\triangle t^{\mathrm{RE}} = 5$.
u, v	Index for wind power time period, $u, v = 1, 2, ..., L$.
w	Index for wind turbines, $w = 1, ..., NW$.
ACE_{CPS2}	The sum of instantaneous ACE until the 10-minute CPS2 interval (L10) ends.
$C_i^{t^{(\cdot)}}$	Operation cost of thermal unit i during period t^{DU}, t^{RU}, and t^{RE}, in \$.
$CPS2_{\mathrm{score}}$	The percent of intervals without violations which take place when an interval exceeds the 50 MW-10 min ACE limit in a 10-minute CPS2 interval.
J	Maximum objective function of the dynamic programming.
L	Number of wind power data points. In DU model, $L = 24$; in RU model, $L = 96$; and in RE model, $L = 288$.
M	Number of WPRP.
NB	Number of buses.

Manuscript received July 6, 2016; revised October 3, 2016 and November 12, 2016; accepted December 31, 2016. Date of publication January 4, 2017; date of current version June 17, 2017. This work was supported by the National Renewable Energy Laboratory under Subcontract XGJ-6-62183-01 (under the U.S. Department of Energy Prime Contract DE-AC36-08GO28308). Paper no. TSTE-00515-2016.

M. Cui and J. Zhang are with the Department of Mechanical Engineering, University of Texas at Dallas, Richardson, TX 75080 USA (e-mail: mingjian.cui@utdallas.edu; jiezhang@utdallas.edu).

H. Wu is with the Department of Electrical and Computer Engineering, Kansas State University, Manhattan, KS 66506 USA (e-mail: hongyuwu@ksu.edu).

B.-M. Hodge is with the National Renewable Energy Laboratory, Golden, CO 80401 USA (e-mail: bri.mathias.hodge@nrel.gov).

Color versions of one or more of the figures in this paper are available online at http://ieeexplore.ieee.org.

Digital Object Identifier 10.1109/TSTE.2017.2647781

NI Number of thermal units.
NL Number of transmission lines.
NW Number of wind turbine generators.
$P_i^{\max}$, $P_i^{\min}$ Max/min generation of unit i, in MW.
R_i^{up}, R_i^{dn} Maximum ramp up/down capability of thermal unit i, in MW/min.
$R(u, v)$ Wind power ramps definition rule of the time interval (u, v).
$S_i^{t^{(\cdot)}}$ Start-up cost of thermal unit i during period t^{DU}, t^{RU}, and t^{RE}, in \$.
$S(u, v)$ Score function of the time interval (u, v).
$T^{(\cdot)}$ Number of time periods. $T^{\mathrm{DU}} = 24$ with 1-hour time resolution in DU model; $T^{\mathrm{RU}} = 4$ with 15-minute time resolution in RU model; and $T^{\mathrm{RE}} = 3$ with 5-minute time resolution in RE model.
$UP^w_{t^{(\cdot)}}$, $DP^w_{t^{(\cdot)}}$ Up/down wind power ramping product of wind turbine w during period t^{DU}, t^{RU}, and t^{RE}, in MW.
$UR_{t^{(\cdot)}}$, $DR_{t^{(\cdot)}}$ Total flexible up/down ramping reserve requirements of thermal units during period t^{DU}, t^{RU}, and t^{RE}, in MW.
$\gamma^{\mathrm{reg}}_{i,t^{(\cdot)}}$, $\gamma^{\mathrm{rep}}_{i,t^{(\cdot)}}$ Bidding price of regulation and replacement reserves of thermal unit i during period t^{DU}, t^{RU}, and t^{RE}, in \$/MWh.
$\gamma^{\mathrm{sp}}_{i,t^{(\cdot)}}$, $\gamma^{\mathrm{ns}}_{i,t^{(\cdot)}}$ Bidding price of spinning and non-spinning reserves of thermal unit i during period t^{DU}, t^{RU}, and t^{RE}, in \$/MWh.
$\gamma^{\mathrm{up}}_{i,t^{(\cdot)}}$, $\gamma^{\mathrm{dn}}_{i,t^{(\cdot)}}$ Bidding price of flexible up/down ramping reserves of thermal unit i during period t^{DU}, t^{RU}, and t^{RE}, in \$/MWh.
ε Only tunable parameter in the OpSDA.
$\underline{\xi}$ Time interval sets of WPRs.
$\overline{\xi}$ Time interval sets of non-WPRs.
σ_{ACE} Standard deviation of area control error.
Θ Time interval sets of WPRP and non-WPRP.

C. Variables

$fu_i^{t^{(\cdot)}}$, $fd_i^{t^{(\cdot)}}$ Scheduled flexible up/down ramping reserves of thermal unit i during period t^{DU}, t^{RU}, and t^{RE}, in MW.
$p_i^{t^{(\cdot)}}$ Dispatch of thermal unit i at the end of period t^{DU}, t^{RU}, and t^{RE}, in MW.
$rg^{t^{(\cdot)}}_{\mathrm{U},i}$, $rg^{t^{(\cdot)}}_{\mathrm{D},i}$ Upward and downward regulation reserves of thermal unit i during period t^{DU}, t^{RU}, and t^{RE}, in MW.
$rp_i^{t^{(\cdot)}}$ Replacement reserves of thermal unit i during period t^{DU}, t^{RU}, and t^{RE}, in MW.
$sp_i^{t^{(\cdot)}}$, $ns_i^{t^{(\cdot)}}$ Spinning and non-spinning reserves of thermal unit i during period t^{DU}, t^{RU}, and t^{RE}, in MW.
$u_i^{t^{(\cdot)}}$ 1 if unit i is scheduled on during period t^{DU}, t^{RU}, and t^{RE}; and 0 otherwise.
$\underline{E_{(\cdot)}}$ Time interval of a WPRP.
$\overline{E_{(\cdot)}}$ Time interval of a non-WPRP.
ρ Percentage of up/down ramping reserve requirement accounting for load.

I. Introduction

THE addition of large amounts of wind power into the power system increases the variability of the netload, which is the load after distributed generation is subtracted out. Two consequences seen at high penetrations of renewable resources are: 1) increased amounts of ramping from online generation units, and 2) possibility of ramp capability shortages. Multiple independent system operators (ISOs) have proposed flexible ramping products to improve the market dispatch flexibility and to address the operational challenges of maintaining power balance [1]–[3], with high levels of variable and uncertain renewable energy generation. For example, the California Independent System Operator (CAISO) has investigated designing a market for up and down flexible ramping services, mainly provided by thermal generators.

A number of researchers have also studied the needs and designs of the flexible ramping product. Marneris *et al.* [4] allowed for the optimal procurement of flexible ramping product on an intra-hourly basis and proposed a probabilistic method for the quantification of flexibility requirements. Xu and Tretheway [1] designed up and down flexible ramping products to address operational challenges of maintaining power balance in the real-time dispatch. Wu *et al.* [5] modeled flexible up/down ramping capability of thermal units to respond to hourly load, and found that flexible ramping would reduce renewable energy curtailments. Navid *et al.* [6] suggested that existing generators of all types maximized the availability of their operational load-following ramp flexibility, and also suggested introducing new flexible ramp suppliers such as demand response. Wang and Hobbs [7], [8] assumed that the purpose of a flexible ramping product market was to manage the increasing load ramp events resulting from the growth in renewable energy, and illustrated that flexible ramping product could enhance market efficiency. Ela *et al.* [9] showed that an up-ramping and a down-ramping product market could be established to cope with load ramps.

However, with the increasing wind power ramps (WPRs) occurring in power systems, there are two critical questions for balancing authorities to pay more attention. First, can balancing authorities rely on wind to provide ramping service, assuming that short-term wind generation and wind power ramps can be forecasted accurately? Second, can balancing authorities design a new ramping product for the system so that the market paradigm can better accommodate wind to provide flexible ramping services? Toward this end, this paper aims to develop an innovative and integrated approach to allow wind power to participate in the flexible ramping market. We propose a wind power ramping product (WPRP) to respond to the need for new ramping services that are being implemented by balancing authorities to ensure that sufficient ramping is available during real-time operations. The purpose of developing a wind-friendly flexible ramping product is to take advantage of the natural wind power ramps. These wind power ramps are typically known for negative characteristics: large fluctuations (significant increase or decrease) of wind power in a short time period. The wind integration cost can be further reduced if we can reasonably forecast wind ramps that could provide ramping service. Two

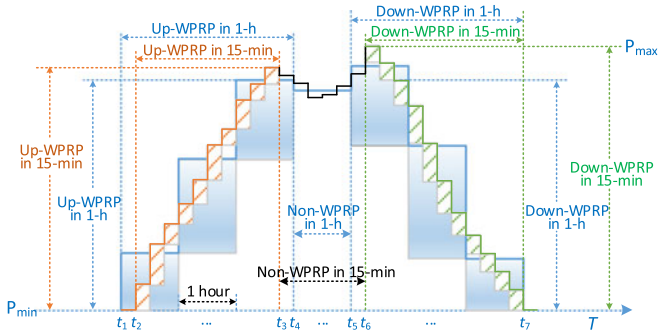

Fig. 1. WPRP performance in the multi-timescale operations using the stair-step graph.

key points in developing WPRP include: (i) how WPRP quantitatively impacts the up- and down-ramping reserve schedules and the production costs; and (ii) how WPRP behaves under different ramping reserve requirements and wind power forecasts. To address these challenges, we develop a ramp detection method to identify WPRs and a modified multi-timescale model that considers WPRP. Note that ramping capacity consists of the "ramping reserve" provided by both thermal generation and wind power, and the wind portion is termed as "wind power ramping product (WPRP)".

The main contribution of this paper is: (i) the design of a wind-friendly flexible ramping product; and (ii) the integration of the wind power ramping product in multi-timescale power system operations. This is a novel contribution because it allows for understanding the full impact of flexible ramping product on practical representations of the state of the art in ISO system operations.

The organization of this paper is as follows. In Section II, a wind-friendly flexible ramping product design method is briefly introduced. In Section III, the modified multi-timescale formulation that considers the wind-friendly flexible ramping product is presented. Case studies and results performed on the modified IEEE 118-bus systems are described in Section IV. Concluding remarks and future work are discussed in Section V.

II. Flexible Wind Power Ramping Product Design

A. Features of WPRP in the Multi-Timescale Operation

Wind power ramps usually show different characteristics in the multi-timescale power system operations, including ramping starts, ramping magnitudes, and ramping durations. In this paper, WPRP is designed to take advantage of the features of WPRs and provide ramping reserves in a positive manner. Fig. 1 exhibits a multi-timescale WPRP detection. The rectangle represents the ramping product that can be provided by wind power at the current time. The first three blue rectangles consist of one up-WPRP with the ramping start time t_1 and ramping end time t_4 in the 1-hour-timescale. The up-WPRP in the 15-minute-timescale model starts at time t_2 ($= t_1 + 15$ min) and terminates at time t_3 ($= t_4 - 15$ min). Moreover, the ramping capacity in the 15-minute-timescale model is much less than that in the 1-hour-timescale model, according to the areas of blue and yellow rectangles. The same phenomenon can also be found

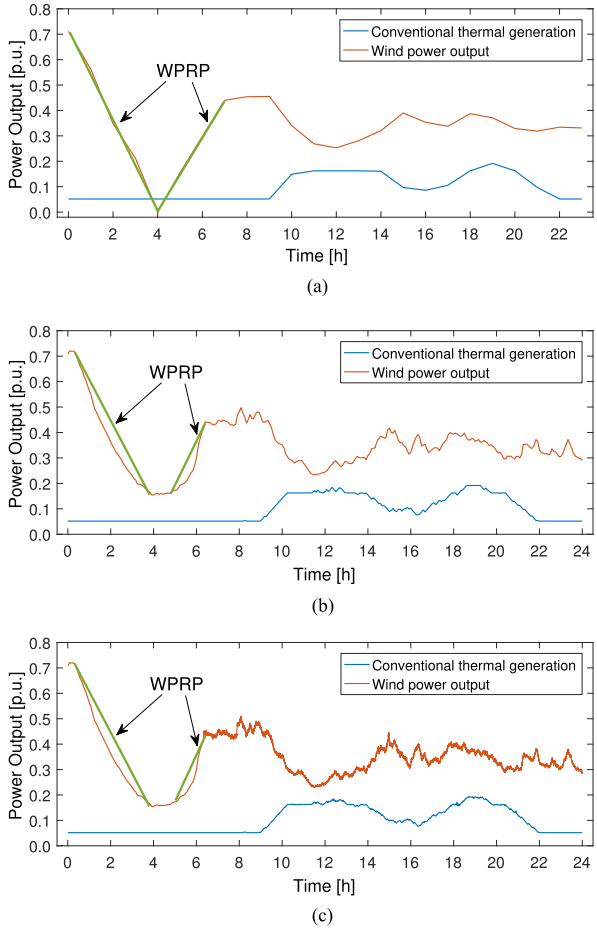

Fig. 2. WPRP performance in the multi-timescale power system operations using line plots. (a) Day-ahead schedules in the unit commitment sub-model (1-hour time resolution). (b) Real-time schedules in the economic dispatch sub-model (5-minute time resolution). (c) Actual generation in the automatic generation control sub-model (6-second resolution).

in the down-WPRP (time $t_5 \sim t_7$ and time $t_6 \sim t_7$). Under this circumstance, it is essential to characterize and consider WPRP features in a multi-timescale fashion. Taking one day as an example, the WPRP performance in the 1-hour, 5-minute, and 6-second timescale operations is illustrated in Fig. 2.

B. Wind Power Ramping Product Design Methodology

The optimized swinging door algorithm (OpSDA) [10] is used to design wind power ramping product at each timescale. In OpSDA, the swinging door algorithm with a predefined parameter ε is first applied to segregate the wind power signal into multiple discrete segments. Then dynamic programming is used to merge adjacent segments with the same ramping direction and relatively high ramping rates [11]. A brief description of OpSDA is introduced here and more details can be found in [10]. Subintervals that satisfy the ramping rules are rewarded by a score function; otherwise, their score is set to zero. The current subinterval is retested as above after being combined with the next subinterval. This process is performed recursively to the end of dataset. Finally, a significant WPRP with the maximum score is extracted. A positive score function, S, is designed based on

the length of the interval segregated by the swinging door algorithm. Given a time interval (u, v) of all discrete time points and an objective function, J, of the dynamic programming, a WPRP is designed by maximizing the objective function, J:

$$J(u,v) = \max_{u<k<v} [S(u,k) + J(k,v)], \quad u < v \tag{1}$$

s.t.

$$S(u,v) > S(u,k) + S(k+1,v), \quad \forall u < k < v \tag{2}$$

$$S(u,v) = (u-v)^2 \times R(u,v) \tag{3}$$

where the positive score function S conforms to a superadditivity property in (2). Ramping rule is defined as the change in wind power magnitude without ramping duration limits [12], [13]. Based on (1)–(3), the optimization process can proceed recursively as follows. Assuming that the number of WPRP is M ($\forall m : 1 < m < M$); the WPRP interval set $\xi = \{E_1, \ldots, E_m, \ldots, E_M\}$ is the set of intervals, $E_m = (s_m, e_m)$; and the non-WPRP interval set $\bar{\xi} = \{\overline{E_1}, \ldots, \overline{E_m}, \ldots, \overline{E_M}\}$ is the set of intervals $\overline{E_m} = (\overline{s_m}, \overline{e_m})$. For $\forall(\overline{s_m}, \overline{e_m}) \in \bar{\xi}$ and $\forall u, v : \overline{s_m} < u < v < \overline{e_m}$, then:

$$R(u,v) = 0 \tag{4a}$$

$$S(u,v) = 0 \tag{4b}$$

$$J^*(\overline{s_m}, \overline{e_m}) = 0 \tag{4c}$$

Considering the super-additivity property in (2), $J^*(s_m, e_m)$ equals $S(s_m, e_m)$. An optimal sequence of WPRP and non-WPRP can be presented as $\Theta = \{\overline{E_1}, E_1, \ldots, \overline{E_m}, E_m, \overline{E_{m+1}}, E_{m+1}, \ldots, E_{M-1}, \overline{E_M}\}$, for a given wind power series with L points. The solution to (1) being $J^*(\overline{s_1}, \overline{e_M})$ is shown in (5). Eqn. (6)–(7) are shown at the bottom of the page.

$$\begin{aligned} J^*(\overline{s_1}, \overline{e_M}) = & \max_{\overline{s_1}<k_1<k_2<\cdots<k_{u-1}<k_u<\overline{e_M}} \{S(\overline{s_1}, k_1) \\ & + S(k_1+1, k_2) + \cdots + S(k_{u-1}+1, k_u)\} \\ & + \max_{k_u+1<k_u<\overline{e_M}} J(k_u+1, \overline{e_M}) \end{aligned} \tag{5}$$

A brief comparison of the swinging door algorithm (SDA) [14], the L1-Ramp Detect with Sliding Window (L1-SW) [11], and the OpSDA [10] is illustrated in Fig. 3. The only tunable parameter, ε, in the SDA and OpSDA is set to 9×10^{-3} [p.u.]. The penalty parameter and the second derivative threshold in L1-SW are set to 0.02 [p.u.] and 5×10^{-6} [p.u.], respectively. It is shown in Fig. 3(a) that the SDA only detects one wind ramp without any optimization. L1-SW detects three wind ramps but the start and terminal points are not always accurate, as shown in Fig. 3(b). The OpSDA in Fig. 3(c) combines the adjacent segments in the same direction and detects the wind ramps more accurately. A detailed description of OpSDA can be found in [10]. The impact of time resolution on wind power ramping has also been studied extensively in [10].

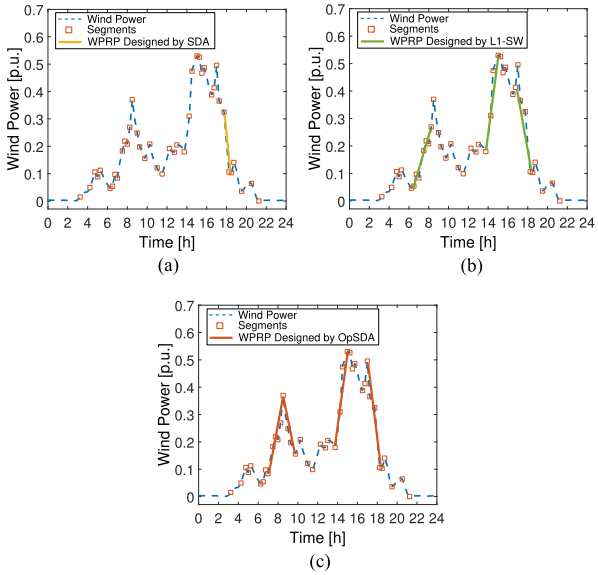

Fig. 3. Comparing wind ramps detection using SDA, L1-SW, and OpSDA. (a) SDA. (b) L1-SW. (c) OpSDA.

III. Multi-Timescale Scheduling Models

To study the impact of WPRP on power system operations, we develop a multi-timescale scheduling method based on a simulation tool, Flexible Energy Scheduling Tool for Integration of

$$\min \sum_{t^{(\cdot)}=1}^{T^{(\cdot)}} \left\{ \sum_{i=1}^{NI} \left[\underbrace{C_i^{t^{(\cdot)}}(p_i^{t^{(\cdot)}}, u_i^{t^{(\cdot)}}) + S_i^{t^{(\cdot)}}(u_i^{t^{(\cdot)}}, u_i^{t^{(\cdot)}-1})}_{\text{Operation and Start-up Cost}} \right.\right.$$
$$\left.\left. + \underbrace{\gamma^{\text{sp}}_{i,t^{(\cdot)}} sp_i^{t^{(\cdot)}} + \gamma^{\text{ns}}_{i,t^{(\cdot)}} ns_i^{t^{(\cdot)}} + \gamma^{\text{rg}}_{i,t^{(\cdot)}} rg_{\text{U},i}^{t^{(\cdot)}} + \gamma^{\text{rg}}_{i,t^{(\cdot)}} rg_{\text{D},i}^{t^{(\cdot)}} + \gamma^{\text{rp}}_{i,t^{(\cdot)}} rp_i^{t^{(\cdot)}}}_{\text{Conventional Reserve Cost}} + \underbrace{\gamma^{\text{up}}_{i,t^{(\cdot)}} fu_i^{t^{(\cdot)}} + \gamma^{\text{dn}}_{i,t^{(\cdot)}} fd_i^{t^{(\cdot)}}}_{\text{Ramping Reserve Cost}} \right] \right\} \tag{6}$$

$$\min \sum_{t^{\text{RE}}=1}^{T^{\text{RE}}} \left\{ \sum_{i=1}^{NI} \left[\underbrace{C_i^{t^{\text{RE}}}(p_i^{t^{\text{RE}}})}_{\text{Operation Cost}} + \underbrace{\gamma^{\text{sp}}_{i,t^{\text{RE}}} sp_i^{t^{\text{RE}}} + \gamma^{\text{ns}}_{i,t^{\text{RE}}} ns_i^{t^{\text{RE}}} + \gamma^{\text{rg}}_{i,t^{\text{RE}}} rg_{\text{U},i}^{t^{\text{RE}}} + \gamma^{\text{rg}}_{i,t^{\text{RE}}} rg_{\text{D},i}^{t^{\text{RE}}} + \gamma^{\text{rp}}_{i,t^{\text{RE}}} rp_i^{t^{\text{RE}}}}_{\text{Conventional Reserve Cost}} \right.\right.$$
$$\left.\left. + \underbrace{\gamma^{\text{up}}_{i,t^{\text{RE}}} fu_i^{t^{\text{RE}}} + \gamma^{\text{dn}}_{i,t^{\text{RE}}} fd_i^{t^{\text{RE}}}}_{\text{Ramping Reserve Cost}} \right] \right\} \tag{7}$$

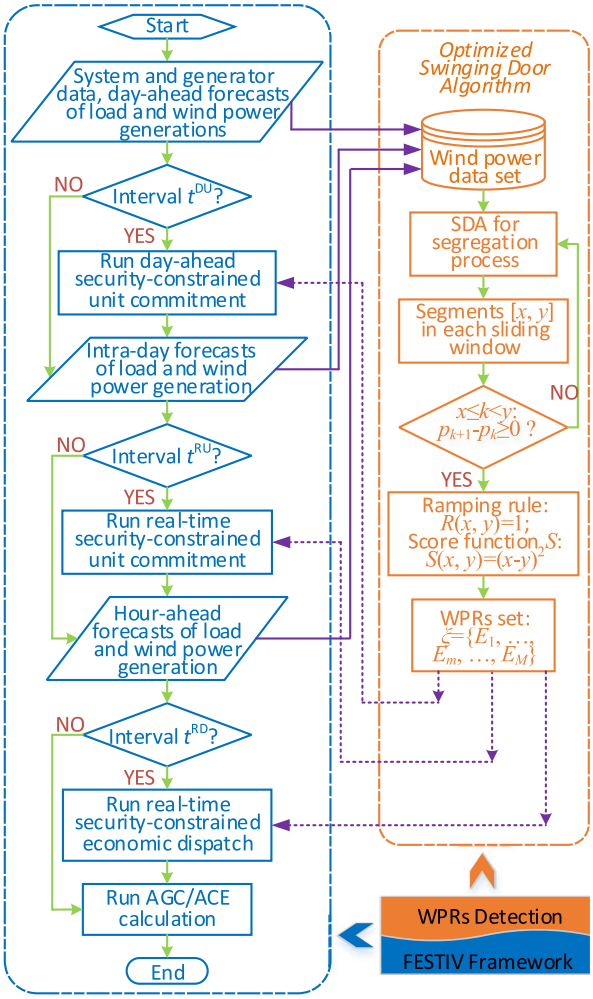

Fig. 4. Multi-timescale scheduling models based on FESTIV with OpSDA.

Variable Generation (FESTIV) [15], [16]. FESTIV is a multi-timescale steady-state power system operations simulation tool that consists of four sub-models: day-ahead security-constrained unit commitment (DASCUC), real-time security-constrained unit commitment (RTSCUC), real-time security-constrained economic dispatch (RTSCED), and automatic generation control (AGC), as shown in the left block of Fig. 4. In this paper, WPRP is designed and considered in each dispatch stage, which is integrated into FESTIV based on the detected ramp results by OpSDA, as shown in the right block of Fig. 4.

A. Objective Functions

In this section, we utilize the formulation proposed by CAISO to add the bid costs from the flexible ramping reserve in thermal generators [1]. The objective function consists of the operation cost, start-up cost, conventional reserve cost, and flexible ramping reserve cost. A piecewise linear approximation of the cost curves of generators is utilized to retain a mixed-integer linear programming (MILP) formulation. The objective function of DASCUC and RTSCUC is stated in (6), where $t^{(\cdot)}$ is t^{DU} or t^{RU} in the day-ahead or real-time security-constrained unit commitment model. The objective function of RTSCED is stated in (7), where the generator status is fixed by the RTSCUC sub-model.

B. Modified Constraints

The objective functions in the FESTIV-OpSDA model comply with a number of constraints defined according to the CAISO model. Prevailing RTSCUC and RTSCED models share similar non-integer constraints. The regulation reserve is supplied in both the upward and downward operating directions with the same attributes whereas the spinning, non-spinning, and replacement reserves are supplied only in the upward operating direction. The main modification in this paper includes ramping capacity limits, active power limits, and flexible ramping requirements, which are stated as follows.

Active power maximum limit:

$$p_i^{t^{(\cdot)}} + \underline{fu_i^{t^{(\cdot)}}} + sp_i^{t^{(\cdot)}} + ns_i^{t^{(\cdot)}} + rg_{\mathrm{U},i}^{t^{(\cdot)}} + rp_i^{t^{(\cdot)}} \le P_i^{\max} \times u_i^{t^{(\cdot)}}, \quad \forall i, \forall t^{(\cdot)} \tag{8}$$

Active power minimum limit:

$$p_i^{t^{(\cdot)}} - \underline{fd_i^{t^{(\cdot)}}} - rg_{\mathrm{D},i}^{t^{(\cdot)}} \ge P_i^{\min} \times u_i^{t^{(\cdot)}}, \quad \forall i, \forall t^{(\cdot)} \tag{9}$$

where (8) represents the active power maximum limit that only considers flexible upward ramping reserve of thermal generators. Likewise, (9) represents the active power minimum limit that only considers flexible downward ramping reserve.

Up-ramping capacity limit:

$$\underline{fu_i^{t^{(\cdot)}}} + sp_i^{t^{(\cdot)}} + ns_i^{t^{(\cdot)}} + rg_{\mathrm{U},i}^{t^{(\cdot)}} + rp_i^{t^{(\cdot)}} \le R_i^{\mathrm{up}} \times \triangle t^{(\cdot)}, \ \forall i, \forall t^{(\cdot)} \tag{10}$$

Constraint (10) ensures that a generator's upward ramping reserve plus the total amount of upward reserve (up-regulation, spinning, and non-spinning) does not exceed the corresponding upward ramping capability over the multi-timescale scheduling interval.

Down-ramping capacity limit:

$$\underline{fd_i^{t^{(\cdot)}}} + rg_{\mathrm{D},i}^{t^{(\cdot)}} \le R_i^{\mathrm{dn}} \times \triangle t^{(\cdot)}, \quad \forall i, \forall t^{(\cdot)} \tag{11}$$

Constraint (11) ensures that a generator's downward ramping reserve plus the down-regulation reserve does not exceed the corresponding downward ramping capability over the multi-timescale scheduling interval.

Upward flexible ramping reserve requirement:

$$\underline{\sum_{i=1}^{NI} fu_i^{t^{(\cdot)}}} + \underbrace{\sum_{w=1}^{NW} UP_{t^{(\cdot)}}^{w}}_{\mathrm{WPRP}} \ge UR_{t^{(\cdot)}}, \quad \forall i, \forall t^{(\cdot)} \tag{12}$$

Upward wind power ramping product:

$$UP_{t^{(\cdot)}}^{w} = \begin{cases} \max\{[p_{t^{(\cdot)}+\Delta t^{(\cdot)}}^{w} - p_{t^{(\cdot)}}^{w}],\ 0\}, & t^{(\cdot)} \in \xi \\ 0, & t^{(\cdot)} \in \overline{\xi} \end{cases} \tag{13}$$

Downward flexible ramping reserve requirement:

$$\underbrace{\sum_{i=1}^{NI} fd_i^{t^{(\cdot)}}} + \underbrace{\sum_{w=1}^{NW} DP_{t^{(\cdot)}}^{w}}_{\text{WPRP}} \geq DR_{t^{(\cdot)}}, \quad \forall i, \forall t^{(\cdot)} \tag{14}$$

Downward wind power ramping product:

$$DP_{t^{(\cdot)}}^{w} = \begin{cases} \max\{[p_{t^{(\cdot)}}^{w} - p_{t^{(\cdot)}+\Delta t^{(\cdot)}}^{w}],\ 0\}, & t^{(\cdot)} \in \xi \\ 0, & t^{(\cdot)} \in \overline{\xi} \end{cases} \tag{15}$$

The same rules for designing the system ramping requirements are adopted in this paper to calculate the wind power ramping product values in constraints (13) and (15). More detailed information about how to design the system ramping requirements can be found in [1].

Additionally, each unit is subject to its own operating constraints, including minimum up and down time constraints, ramping rate constraints, and initial condition constraints. For the sake of simplicity, the aforementioned constraints are not listed specifically in this paper as they are common among many unit commiment and economic dispatch models [17], [18]. The main contribution of this work is to develop and integrate flexible ramping reserve into FESTIV, including the objective function ($\gamma_{i,t^{(\cdot)}}^{\text{up}} fu_i$ and $\gamma_{i,t^{(\cdot)}}^{\text{dn}} fd_i$ in (6) and (7)), power output limits, ramping capacity limits, and ramping requirement constraints in (8)–(14). Moreover, both wind power up- and down-ramping product are considered in formulating and examining constraints (12) and (14).

C. Description of the Reliability Indicators

In addition to the common economic indicators (reserve, operation, and production costs), we also compare reliability metrics for cases with WPRP and without WPRP based on the system's area control error (ACE) and the Control Performance Standard 2 (CPS2) proposed by the North American Electric Reliability Corporation (NERC) [19], [20]. ACE is the difference between the sum of total generation and load at any time, which is the main driver of all imbalance metrics, the formula for which is:

$$ACE_t = K_1 ACE_{t,\text{inst}} + \frac{K_2}{T_n} \int_{t-T_n}^{t} ACE_{\tau,\text{inst}} d\tau \tag{16}$$

where ACE_t is the smoothed ACE value of the system at time period t. $ACE_{t,\text{inst}}$ represents the instantaneous ACE value at time period t. The term τ is the index for time intervals. The terms T_n, K_1, and K_2 are parameters used for the smoothed AGC mode.

Absolute area control error in energy (AACEE) is the absolute value of ACE at every t_{AGC} interval, where t_{AGC} is the highest time resolution (in seconds) at which AGC is run. AACEE is a function of the time resolution of the RTSCED (I_{RTD}), the time horizon of the RTSCED (H_{RTD}), the amount of wind power on the system (P_{WIND}), the load (P_{LOAD}), and the amount of total ramping available from the resources to manage the variability (P_{RAMP}), formulated as:

$$\begin{aligned} AACEE = {} & \alpha_1 I_{\text{RTD}} + \alpha_2 H_{\text{RTD}} + \alpha_3 P_{\text{WIND}} \\ & + \alpha_4 P_{\text{LOAD}} + \alpha_5 P_{\text{RAMP}} \end{aligned} \tag{17}$$

where α is the sensitivity coefficient and can be calculated from the standard deviation of output changes at different timescales, i.e., $\alpha_1 = \partial AACEE/\partial I_{\text{RTD}}$; $\alpha_2 = \partial AACEE/\partial H_{\text{RTD}}$; $\alpha_3 = \partial AACEE/\partial P_{\text{WIND}}$; $\alpha_4 = \partial AACEE/\partial P_{\text{LOAD}}$; and $\alpha_5 = \partial AACEE/\partial P_{\text{RAMP}}$.

Control Performance Standard 2 (CPS2) is a NERC reliability standard that measures the amount of intervals where the absolute value of ACE exceeds a predefined threshold [21]. Based on CPS2, the reliability indicator ACE_{CPS2} measures the sum of instantaneous ACE until the 10-minute CPS2 interval (L10) ends for use in calculating $CPS2_{\text{score}}$. Thus the unit of ACE_{CPS2} is MW-10 min and the τth ACE_{CPS2} is formulated as:

$$ACE_{\text{CPS2},\tau} = \sum_{t=(\tau-1)\times T_{\text{CPS2}}\times 60}^{\tau \times T_{\text{CPS2}} \times 60 - t_{\text{AGC}}} ACE_{t,\text{inst}} \times \frac{t_{\text{AGC}}}{T_{\text{CPS2}} \times 60} \tag{18}$$

where T_{CPS2} is the CPS2 interval, i.e., 10 minutes. τ is the index of the τth ACE_{CPS2} value.

$CPS2_{\text{score}}$ measures the percentage of intervals without violations that take place when an interval exceeds the 50 MW-10 min ACE limit in a 10-minute CPS2 interval (L10). This gives an indication of how often the system encounters severe imbalance errors. A flag variable f_τ is defined to indicate whether the $CPS2_{\text{score}}$ exceeds the 50 MW-10 min ACE limit:

$$f_\tau = \begin{cases} 1, & \text{if } ACE_{\text{CPS2},\tau} > 50 \\ 0, & \text{if } ACE_{\text{CPS2},\tau} \leq 50 \end{cases} \tag{19}$$

Thus, the CPS2 score ($CPS2_{\text{score}}$) is defined as:

$$CPS2_{\text{score}} = \left(1 - \frac{N_{\text{V}}}{N_{\text{T}}}\right) \times 100 \tag{20}$$

where N_{T} is the number of total periods. N_{V} is the number of violation periods and $N_{\text{V}} = \sum f_\tau$.

Overall, it should be highlighted that a higher $CPS2_{\text{score}}$ and lower ACE, AACEE, and ACE_{CPS2} scores indicate better performance in terms of the reliability indicators.

IV. Case Studies and Results

A. Test Cases

We perform numerical simulations using the FESTIV-OpSDA model on a modified IEEE 118-bus system. Detailed description and results of numerical simulations on a modified PJM (Pennsylvania-New Jersey-Maryland Interconnection) 5-bus system can be found in [22]. All tests are carried out using the General Algebraic Modeling System (GAMS) Distribution 24.7 [23], and solved using ILOG CPLEX 12.6 [24] on an Intel-e5-2603 1.6-GHz workstation with 32 GB of RAM memory. The modified IEEE 118-bus system is performed in the developed FESTIV-OpSDA model to show the effectiveness of WPRP with different wind power penetration levels and ramping reserve requirements. This system has 54 thermal units, 186 branches, and 91 load buses. The parameters of generators, transmission network, and load profiles are given in [25], [26]. All ancillary services, including spinning, non-spinning, regulation, replacement, and up/down ramping reserves, are considered. The system peak demand is 4,064 MW at the time stamp

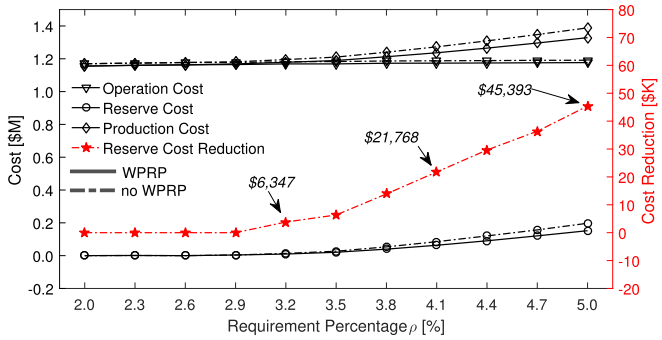

Fig. 5. Costs comparison of increasing ramping reserve requirements.

18:46:24. There is one wind generator connected to Bus 43. In this system, we use four wind power penetration levels (6.99%, 13.55%, 20.12%, and 26.70%) as different simulation scenarios. Four cases are performed to validate the analysis. The first two cases are to study the impacts of different ramping reserve requirements and wind power penetrations. We perform a third case to analyze the reliability impact of WPRP on system operations. The first three cases use the perfect wind power forecast, i.e., actual wind power. The last case analyzes the impact of wind power forecasting accuracy on WPRP and ramping services using different weekly wind power forecasting data.

B. Comparison of WPRP With Increasing Ramping Reserve Requirements in Terms of Economic Benefits and Generation Schedules

In Fig. 5, we compare the economic impact of considering WPRP when the ramping reserve requirement increases. The simulation time period is one day with the representative peak load. For the simplicity of comparison, it is assumed that the flexible ramping reserve requirement is highly needed for balancing authorities. Thus the ramping reserve requirement is defined as a percentage (2%∼5%) of load in this case. The operation cost remains consistent. The total production costs increase due to the increase of reserve costs. Both total production cost and reserve cost show a linear growth with the increase of ramping reserve requirement. When the requirement percentage ρ equals 3.2%, the saved reserve cost considering WPRP is \$6,347 per day. When ρ equals 4.1%, the saved reserve cost is \$21,768 per day. When ρ equals 5.0%, the saved reserve cost is \$45,393 per day. Saved reserve costs rise significantly after $\rho = 2.9\%$. Almost double reserves held causes more expensive units to schedule online and provide flexible ramping reserves. This shows that WPRP can significantly reduce the reserve cost especially when more ramping reserves are needed.

Fig. 6 compares generation schedules of six representative generators in two cases: (i) Fig. 6(a) by considering WPRP or not, and (ii) Fig. 6(b) by increasing the ramping reserve requirement. There are slight differences considering WPRP or not. Since the power balance between load and generators must be well kept, other 53 generators increase the output to mitigate the relatively big difference during 1h-8h. WPRP doesn't impact the system operation balance.

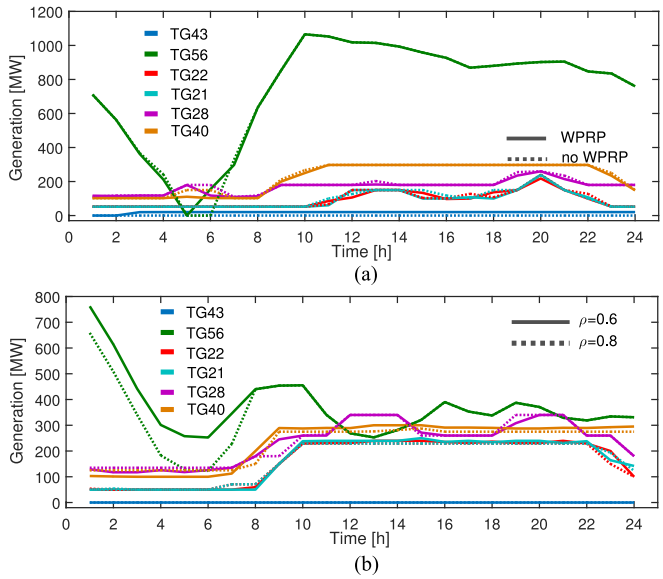

Fig. 6. Generation schedules comparison in two cases. (a) With/without WPRP. (b) Different ramping reserve requirements.

TABLE I
TOTAL SCHEDULED UP- AND DOWN-RAMPING RESERVES OF FOUR SCENARIOS WITH PERFECT WIND POWER FORECAST ($\rho = 5\%$)

Scenarios	Wind Penetration Level	Total Up-Ramping Reserve [MWh]	Total Down-Ramping Reserve [MWh]
SC0 (Benchmark)	non-WPRP	5,040	5,040
SC1	6.99%	**4,951**	**4,832**
SC2	13.55%	4,902	**4,387**
SC3	20.12%	**3,986**	4,773
SC4	26.70%	4,605	4,588

C. Impact of Increasing Wind Penetration Level on Up- and Down-Ramping Reserve Schedules

In Table I, the scenario without WPRP is taken as the benchmark scenario, SC0. SC1 with the smallest wind penetration 6.99% saves the least up-ramping reserve from thermal generators, 89 MW, and down-ramping reserve, 208 MW. The ramping magnitude of WPRP in SC1 is the smallest, as shown by the blue line in Fig. 7. Note that for comparison, WPRP in OpSDA is designed as WPRs with magnitudes larger than 8% of the maximum wind power generation in each scenario instead of the installed capacity or a fixed threshold. Therefore, the most WPRPs are detected in SC1 even with the smallest ramping magnitude. Since dynamic programming merges the adjacent subintervals into one complete WPRP, scenarios SC2, SC3, and SC4 obtain fewer but much larger WPRPs, which would make more sense of providing WPRPs. A more interesting finding is that the smaller wind penetration level can occasionally supply more WPRPs and then save more ramping reserves from thermal generators. For instance, SC3 (20.12% wind penetration) saves more up-ramping reserves, 1,054 MW, compared to SC4 (26.70% wind penetration) with fewer up-ramping reserve

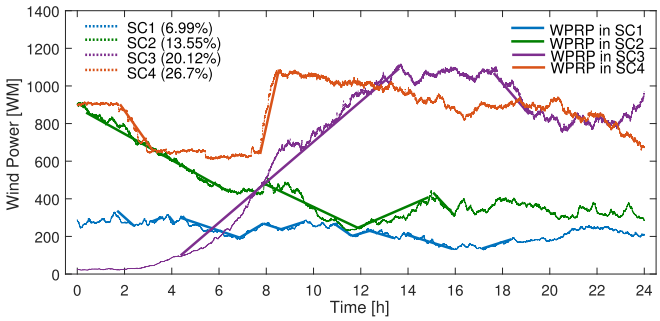

Fig. 7. Four scenarios with different wind penetrations and corresponding WPRP. 5 up-WPRPs and 7 down-WPRPs in SC1; 1 up-WPRP and 3 down-WPRPs in SC2; 1 up-WPRP and 1 down-WPRP in SC3; and 1 up-WPRP and 1 down-WPRP in SC4.

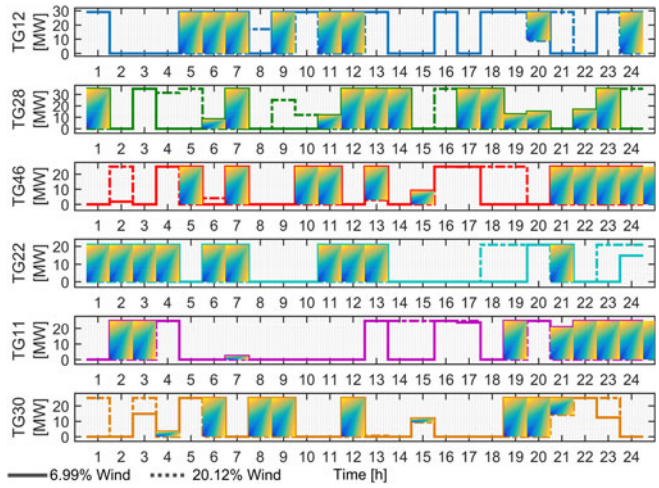

Fig. 8. Up-ramping reserve schedules with two wind penetrations. The rectangles in color are the reduced up-ramping reserve after the wind penetration level increases.

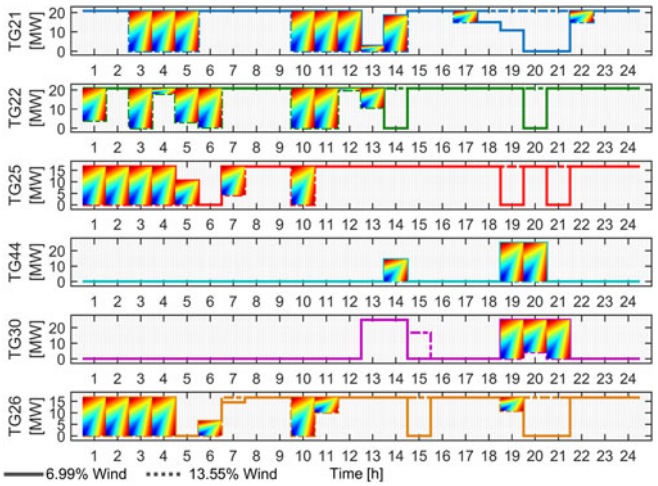

Fig. 9. Down-ramping reserve schedules with two wind penetrations. The rectangles in color are the reduced down-ramping reserve after the wind penetration level increases.

TABLE II
RELIABILITY METRICS FOR FOUR SCENARIOS WITH DIFFERENT PENETRATION LEVELS ($\rho = 5\%$)

Scenarios	AACEE [MWh]		σ_{ACE} [MW]		$CPS2_{\mathrm{score}}$ [%]	
SC1, non-WPRP	96.89	∼	5.17	∼	100	∼
SC1, WPRP	96.89		5.17		100	
SC2, non-WPRP	123.66	↓	7.25	↓	99.21	↑
SC2, WPRP	122.04		7.22		99.65	
SC3, non-WPRP	202.53	↓	11.52	↓	97.91	↑
SC3, WPRP	201.67		11.49		98.74	
SC4, non-WPRP	175.19	↓	10.14	↓	98.45	↑
SC4, WPRP	172.65		10.12		99.31	

saved, 435 MW. Because wind power in SC3 provides the largest up-WPRP as shown by the purple line in Fig. 7. Likewise, SC2 (13.55% wind penetration) saves more down-ramping reserves, 653 MW, than SC4 with fewer down-ramping reserve saved, 452 MW. This is due to the two significant WPRPs that are supplied as ramping reserve in SC2, as shown by the green line in Fig. 7. The uncontrollability of wind power ramps makes it possible that there may be larger WPRPs at a relatively lower wind penetration level (e.g., SC3). It encourages balancing authorities to integrate wind in a more positive manner even at a small penetration level.

Figs. 8 and 9 compare up- and down-ramping reserve schedules in two scenarios, respectively. Scenarios with the most and least ramping reserves are compared, i.e., SC1&SC3 for up-ramping reserve comparison and SC1&SC2 for down-ramping reserve comparison. The top six generators saved with the most ramping reserves are chosen for comparison. It is seen that in most time periods, schedules of both up- and down-ramping reserves significantly decrease, as shown by the rectangles in color. The economic benefits of WPRP are visually illustrated in these two figures.

D. Reliability Impacts of WPRP

The same four scenarios (SC1, SC2, SC3, and SC4) in Section IV-C are performed in this case and the requirement percentage ρ is set as 5%. In Table II, reliability metrics considering WPRP are enumerated based on the absolute ACE in energy (AACEE), the standard deviation of ACE (σ_{ACE}), and the score of CPS2 ($CPS2_{\mathrm{score}}$) metrics. Table II shows that the scenarios considering WPRP perform equal-to-better than those without WPRP in terms of reliability metrics, i.e., smaller ACE values and larger $CPS2_{\mathrm{score}}$. When the wind penetration level is low as seen in SC1 with WPRP, reliability metrics are not affected by using WPRP. However, when the wind penetration level increases, the use of WPRP has shown a better reliability performance, i.e., the decrease of ACE values and the increase of $CPS2_{\mathrm{score}}$. This is because in these cases, WPRP provides extra ramping reserves and reduces the power system imbalance when the system requires more ramping capacity. Moreover, the SC3 scenario shows the lowest $CPS2_{\mathrm{score}}$ due to the most significant up-WPRP as seen in Fig. 7.

The average execution time for the four scenarios with WPRP and without WPRP are compared in Table III. It is shown that the average execution time considering WPRP slightly increases

TABLE III
AVERAGE EXECUTION TIME FOR FOUR SCENARIOS

Scenarios	Execution Time [s]
without WPRP	1,675
with WPRP	1,816

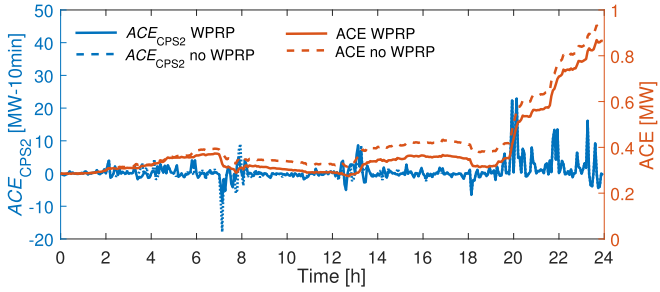

Fig. 10. Reliability impacts on SC4.

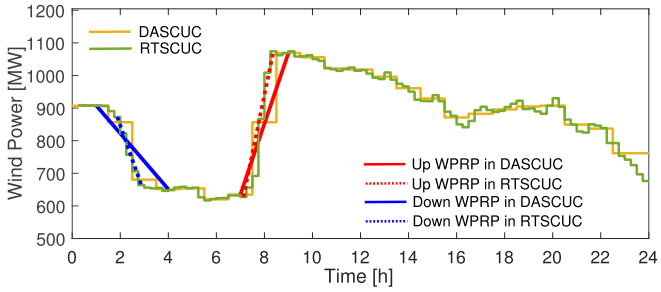

Fig. 11. Designed WPRP based on SC4.

(by ∼2 minutes) due to the process for wind-friendly flexible ramping product design.

As shown in Figs. 10 and 11, we use the DASCUC and RTSCUC models on SC4 scenario to illustrate the detected wind power ramps that are positively regarded as wind power ramping product. Time series of ACE and CPS2 are also plotted with/without WPRP. Fig. 10 indicates that using WPRP can reduce ACE_{CPS2} and the continuous integrated ACE in this case. The volatility of ACE_{CPS2} series gets relatively convergent and stable as shown by the gray dashed line, especially during the time period 7h–9h, which makes $CPS2_{\mathrm{score}}$ increase.

Another interesting finding in Fig. 11 is that WPRP generally behaves relatively arbitrarily in the DASCUC model due to its natural characteristics (i.e., lack of intra-hour information) at the 1-h time resolution. In this case, WPRP is supplied during time intervals 1h–4h and 7h–9h in DASCUC model. While in RTSCUC model, it is supplied at the 15-min time resolution from 2:15 to 3:30 and from 7:30 to 9:00. By extension, the RTSCUC model still uses relatively arbitrary WPRP comparing to the RTSCED model, which has a 5-min time resolution. Since a WPRP can occur and be scheduled at any time interval, a multi-timescale operation model is very necessary and effective for WPRP analysis.

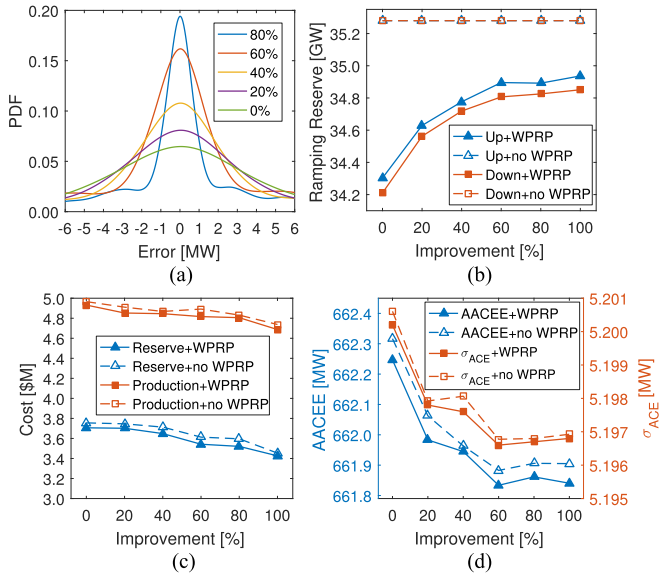

Fig. 12. Impacts of different forecasting improvements with/without WPRP on ramping reserve (b), economic metrics (c), and reliability metrics (d) with a small forecasting error interval from −6 MW to 6 MW.

E. Impact of Wind Power Forecasting Accuracy on Ramping Services

To illustrate the impact of wind power forecasting accuracy on ramping services, two cases have been studied with different forecasting error intervals:

1) *Case 1:* A small forecasting error interval from −6 MW to 6 MW.
2) *Case 2:* A large forecasting error interval from −60 MW to 60 MW.

Case 1: In this case, weekly data with a small forecasting error interval from −6 MW to 6 MW are simulated. Fig. 12 shows how the improvements of wind power forecasting accuracy impact the service of WPRP on power system operations. The wind power forecasts are generated using a predefined normally distributed error that is randomly added to the perfect wind power forecast. This forecast is then taken as the benchmark case (0% improvement). Forecast errors are uniformly decreased by a percentage (20%) to create other improvement scenarios (20%, 40%, 60%, and 80%). The 100% improvement represents the perfect power forecast. The probability distribution functions (PDFs) of forecast errors are shown in Fig. 12(a). Fig. (b) shows that ramping reserves in forecast cases are generally not scheduled enough comparing to the perfect improvement case (100%), since more WPRPs are overestimated by forecasts. Fig. 12(c) indicates that both production and reserve costs are reduced with the increase of wind power forecasting accuracy. Fig. 12(d) illustrates the decreasing AACEE and ACE standard deviation with the increasing forecasting improvement.

In practice, wind power is precontracted to supply the WPRP service based on forecasts. If the contract is made based on the 20% improvement case, there are 307 MWh up-ramping and 288 MWh down-ramping reserves underestimated comparing to the perfect case. This underestimate of ramping services

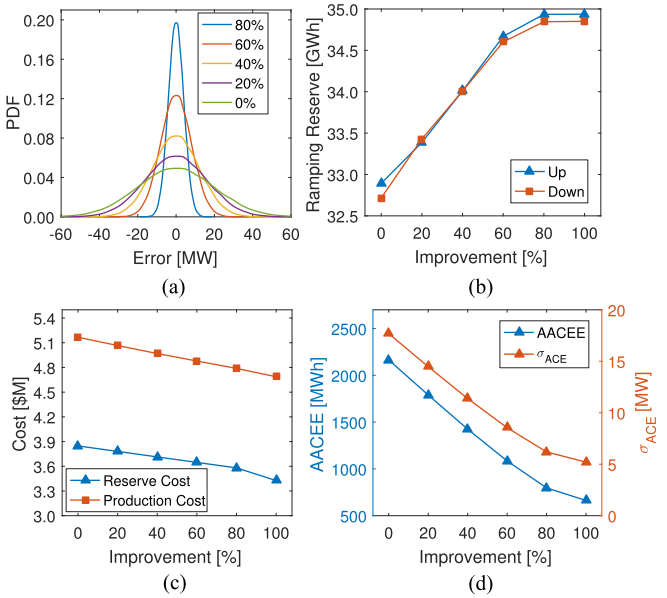

Fig. 13. Impacts of different forecasting improvements on ramping reserve (b), economic metrics (c), and reliability metrics (d) with a large forecasting error interval from −60 MW to 60 MW.

affects both economic and reliability benefits, i.e., the cost increase of production (∼$0.16 M) and reserve (∼$0.27 M), and the control errors increase of AACEE (∼142 KWh) and σ_{ACE} (∼0.99 KW). If the contract is made based on the 60% improvement case, there are only 45 MWh up-ramping and 44 MWh down-ramping reserves underestimated according to the perfect case. The production and reserve costs increase by ∼$0.13 M and ∼$0.12 M, respectively. However, the reliability metrics are almost not affected comparing to the perfect wind power forecast.

Results without WPRP are also compared with the metrics of ramping reserve requirements, economic metrics, and reliability metrics with dashed lines in Fig. 12(b)–(d). It is seen that both economic and reliability indicators are improved after considering the WPRP. Taking the 60% improvement case as an example, the reductions in the reserve cost and the production cost are ∼$70,900 and ∼$75,100, respectively. The reductions in AACEE and σ_{ACE} are ∼49 KW and ∼0.1749 KW, respectively.

Case 2: Weekly data with a large forecasting error interval from −60 MW to 60 MW are simulated for generalized analysis in this case. Wind power forecasts are generated using larger predefined errors as shown in Fig. 13(a). Other improvement scenarios are generated in the same way as in Case 1. With the increase in forecasting errors, WPRPs are overestimated compared to Case 1, which may result in a deficit of ramping reserves scheduled by the system. For example, the benchmark (0% improvement) in Case 1 schedules 34.31 GWh up-ramping and 34.21 GWh down-ramping reserves, whereas the benchmark (0% improvement) in Case 2 schedules only 32.89 GWh up-ramping and 32.72 GWh down-ramping reserves. Both the economic metrics in Fig. 13(c) and the reliability indicators in Fig. 13(d) are increased due to larger forecasting errors. For

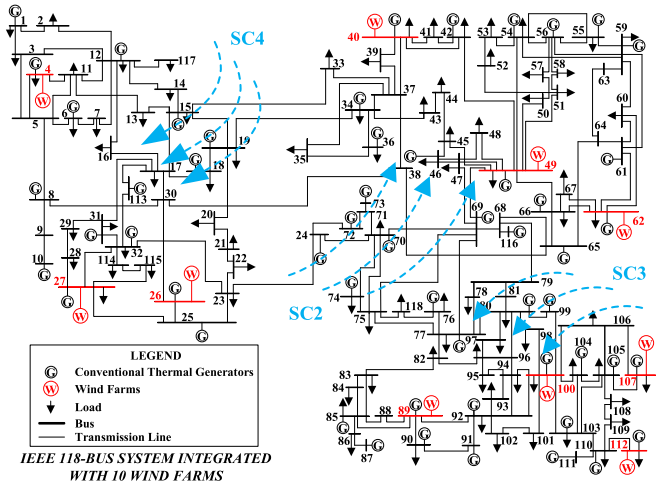

Fig. 14. IEEE 118-bus system integrated with 10 wind farms [27].

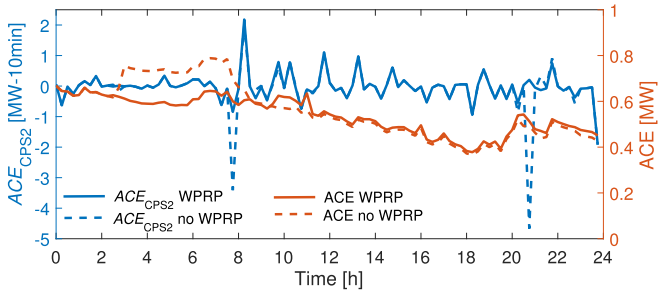

Fig. 15. Comparison of reliability indicators in the IEEE 118-bus system with 10 wind farms.

example, the production cost of the benchmark (0% improvement) is ∼$4.93 M in Case 1 and increases to ∼$5.17 M in Case 2. AACEE of the benchmark (0% improvement) is ∼662 MWh in Case 1 and increases to ∼2,164 MWh in Case 2. Overall, the two case studies considering different levels of forecasting errors have shown the importance of wind power forecasting improvements when designing WPRP to provide ramping services.

F. Allocation of Ten Wind Farms

To present a more realistic renewable-based generation system, the IEEE 118-bus system is modified by allocating 10 wind farms (as shown in Fig. 14) based on the apparent power of the loads and the distance of transmission lines. More detailed information can be found in [27]. Wind power generation of three scenarios (SC2, SC3, and SC4) in Section IV-A are performed as the output of wind farms. For instance, SC4 is the output of wind farms on Bus 4, 26, and 27 in the top left zone. SC2 is the output of wind farms on Bus 40, 49, and 62 in the top right zone. SC3 is the output of wind farms on Bus 89, 100, 107, and 112 in the bottom right zone.

Fig. 15 and Table IV compare the reliability metrics (AACEE, σ_{ACE}, $CPS2_{\mathrm{score}}$, ACE_{CPS2}, and ACE) and economic metrics (operation cost, reserve cost, and production cost) considering the cases with and without considering the

TABLE IV
COMPARISON OF ECONOMIC AND RELIABILITY METRICS IN IEEE 118-BUS SYSTEM WITH 10 WIND FARMS

	Metrics	Without WPRP	With WPRP
Economic	Operation Cost [$M]	1.1148	1.1054
	Reserve Cost [$M]	1.0008	0.1937
	Production Cost [$M]	2.1156	1.2991
Reliability	AACEE [MWh]	100.03	98.77
	σ_{ACE} [MW]	5.41	5.39
	$CPS2_{\mathrm{score}}$ [%]	97.92	99.31

WPRP. In Fig. 15, the curves of ACE_{CPS2} and ACE with the WPRP converge closer to zero with less fluctuation, compared to that without the WPRP. Numerical results of the reliability metrics in Table IV show the decrease of AACEE and σ_{ACE} and the increase of $CPS2_{\mathrm{score}}$, after considering the WPRP. Moreover, the cost metrics are also reduced when considering the WPRP. Overall, the WPRP can provide both economic and reliability benefits to power system operations even when more wind farms are integrated into the grid.

V. CONCLUSION

This paper developed a wind-friendly flexible ramping product and integrated the wind power ramping product (WPRP) into multi-timescale power system operations. The IEEE 118-bus model was modified to evaluate the impacts of the WPRP. A set of case studies were performed to study: (i) the economic benefits of WPRP under different ramping reserve requirements; (ii) the impacts of increasing wind penetration on up- and down-ramping reserve schedules; (iii) the reliability impacts of WPRP under different wind penetration levels; and (iv) the impacts of wind power forecasting accuracy on flexible ramping service.

The optimized swinging door algorithm (OpSDA) was adopted to extract and identify wind power ramps that could be utilized as part of the flexible ramping products. A multi-timescale scheduling method was developed based on an optimization simulation tool, the Flexible Energy Scheduling Tool for Integration of Variable Generation (FESTIV), to integrate and explore the flexible ramping products. Four sub-models with different dispatch stages (1-hour, 15-minute, 5-minute, and 6-second time resolutions) were considered in the multi-timescale system operations, i.e., day-ahead unit commitment, real-time unit commitment, real-time economic dispatch, and automatic generation control (AGC). The objective of the optimization model consisted of the operation cost, start-up cost, conventional reserve cost, and flexible ramping reserve cost. A number of common generation constraints and ramping-related constraints (i.e., ramping capacity limits, active power limits, and flexible ramping requirements) were considered in the multi-timescale power system operations. Numerical results of multiple case studies showed that:

i) The WPRP could significantly decrease both the reserve cost and the total production cost, especially when more ramping reserves were required for power system operations. For instance, when the requirement percentage was 3.2% of load, the reserve cost savings by considering WPRP were $6,347 per day. When the requirement percentage was 5.0% of load, the reserve cost savings were $45,393 per day, for the IEEE 118-bus system.
ii) Both up- and down-ramping reserve schedules of thermal units were significantly reduced after utilizing the WPRP. It was also interesting to find that the 20.12% wind penetration scenario saved more up-ramping reserves, 1,054 MW, compared to the 26.70% wind penetration scenario, 435 MW. The variable and uncertain nature of wind power ramps made it possible that there might be larger WPRPs at a relatively lower wind penetration level, depending on the geographic smoothing of the wind resources represented. This finding could encourage balancing authorities to integrate wind power in a more positive manner even at small penetration levels.
iii) Scenarios considering WPRP performed equal-to-better than those without WPRP in terms of reliability metrics, i.e., smaller ACE values and larger $CPS2_{\mathrm{score}}$. After using the WPRP, the volatility of ACE_{CPS2} series became more convergent and stable, especially during the time period when a large upward wind ramp occurred (i.e., 7 h-9 h), which accordingly increased the $CPS2_{\mathrm{score}}$. The average execution time considering WPRP was slightly increased (by $\sim$2 minutes) due to the additional constraints implemented for the wind-friendly flexible ramping product design.
iv) Wind power forecasting accuracy played a key role in designing the WPRP to provide ramping services. The economic metrics (reserve cost and production cost) and the reliability cost (AACEE and σ_{ACE}) were significantly reduced when the forecasting accuracy was improved.
v) When more wind plants with different power outputs were placed in the IEEE 118-bus system at different buses, both ACE_{CPS2} and ACE converged closer to zero with less fluctuation when considering the WPRP, comparing to the cases without the WPRP. Numerical results quantitatively showed the increase in $CPS2_{\mathrm{score}}$ and the decrease in AACEE, σ_{ACE}, operation cost, reserve cost, and production cost.

In the future, this research can be further improved by: (i) developing probabilistic WPRP that can be used in stochastic power system operation models; and (ii) analyzing the impact of WPRP on the design and management of flexible ramping reserve requirements of conventional generators.

ACKNOWLEDGMENT

The authors would also like to thank the anonymous reviewers for their constructive suggestions to this research.

REFERENCES

[1] L. Xu and D. Tretheway, "Flexible ramping products," *CAISO*, Folsom, CA, USA, 2012.
[2] MISO, "Ramp capability product design for MISO markets," Midcontinent Independent System Operator (MISO), Carmel, IN, USA. 2013, Jul. [Online]. Available: https://www.misoenergy.org/Library/Repository/Communication%20Material/Key%20Presentations%20and%20White papers/Ramp%20Product%20Conceptual%20Design%20Whitepaper.pdf

[3] N. Parker, "Ramp product design." 2015, August 12. [Online]. Available: https://www.spp.org/documents/29342/ramp%20product%20design.pdf
[4] I. G. Marneris, P. N. Biskas, and E. A. Bakirtzis, "An integrated scheduling approach to underpin flexibility in european power systems," *IEEE Trans. Sustain. Energy*, vol. 7, no. 2, pp. 647–657, Apr. 2016.
[5] H. Wu, M. Shahidehpour, A. Alabdulwahab, and A. Abusorrah, "Thermal generation flexibility with ramping costs and hourly demand response in stochastic security-constrained scheduling of variable energy sources," *IEEE Trans. Power Syst.*, vol. 30, no. 6, pp. 2955–2964, Nov. 2015.
[6] N. Navid and G. Rosenwald, "Market solutions for managing ramp flexibility with high penetration of renewable resource," *IEEE Trans. Sustain. Energy*, vol. 3, no. 4, pp. 784–790, Oct. 2012.
[7] B. Wang and B. F. Hobbs, "A flexible ramping product: Can it help real-time dispatch markets approach the stochastic dispatch ideal?" *Elect. Power Syst. Res.*, vol. 109, pp. 128–140, Apr. 2014.
[8] B. Wang and B. F. Hobbs, "Real-time markets for flexiramp: A stochastic unit commitment-based analysis," *IEEE Trans. Power Syst.*, vol. 31, no. 2, pp. 846–860, Mar. 2016.
[9] E. Ela, B. Kirby, N. Navid, and J. C. Smith, "Effective ancillary services market designs on high wind power penetration systems," in *Proc. IEEE Power Energy Soc. Gen. Meet.*, San Diego, CA, USA, 2012, pp. 1–8.
[10] M. Cui, J. Zhang, A. R. Florita, B.-M. Hodge, D. Ke, and Y. Sun, "An optimized swinging door algorithm for identifying wind ramping events," *IEEE Trans. Sustain. Energy*, vol. 7, no. 1, pp. 150–162, Jan. 2016.
[11] R. Sevlian and R. Rajagopal, "Detection and statistics of wind power ramps," *IEEE Trans. Power Syst.*, vol. 28, no. 4, pp. 3610–3620, Nov. 2013.
[12] J. Zhang, A. Florita, B.-M. Hodge, and J. Freedman, "Ramp forecasting performance from improved short-term wind power forecasting," in *Proc. ASME Int. Des. Eng. Tech. Conf. Comput. Inf. Eng. Conf.*, Buffalo, NY, USA, Aug. 2014, Paper DETC2014-34775.
[13] C. Kamath, "Associating weather conditions with ramp events in wind power generation," in *Proc. Power Syst. Conf. Expo.*, Phoenix, AZ, USA, 2011, pp. 1–8.
[14] E. H. Bristol, "Swinging door trending: Adaptive trend recording?" in *Proc. ISA Nat. Conf.*, 1990, pp. 749–753.
[15] Flexible Energy Scheduling Tool for Integrating Variable Generation (FESTIV) Model, 2011. [Online]. Available: http://www.nrel.gov/electricity/transmission/festiv.html.
[16] E. Ela and M. O'Malley, "Studying the variability and uncertainty impacts of variable generation at multiple timescales," *IEEE Trans. Power Syst.*, vol. 27, no. 3, pp. 1324–1333, Aug. 2012.
[17] H. Wu, M. Shahidehpour, A. Alabdulwahab, and A. Abusorrah, "Demand response exchange in the stochastic day-ahead scheduling with variable renewable generation," *IEEE Trans. Sustain. Energy*, vol. 6, no. 2, pp. 516–525, Apr. 2015.
[18] E. Ela, M. Milligan, and M. O'Malley, "A flexible power system operations simulation model for assessing wind integration," in *Proc. IEEE Power Energy Soc. Gen. Meet.*, San Diego, CA, USA, 2011, pp. 1–8.
[19] E. Ela, V. Gevorgian, A. Tuohy, B. Kirby, M. Milligan, and M. O'Malley, "Market designs for the primary frequency response ancillary service–Part I: Motivation and design," *IEEE Trans. Power Syst.*, vol. 29, no. 1, pp. 421–431, Jan. 2014.
[20] E. Ela, V. Gevorgian, A. Tuohy, B. Kirby, M. Milligan, and M. O'Malley, "Market designs for the primary frequency response ancillary service–Part II: Case studies," *IEEE Trans. Power Syst.*, vol. 29, no. 1, pp. 432–440, Jan. 2014.
[21] North American Electric Reliability Corporation. Reliability Standards for the Bulk Electric Systems of North America 2016. [Online]. Available: http://www.nerc.com/pa/Stand/Reliability%20Standards%20Complete%20Se t/RSCompleteSet.pdf
[22] M. Cui, J. Zhang, H. Wu, B.-M. Hodge, D. Ke, and Y. Sun, "Wind power ramping product for increasing power system flexibility," in *Proc. IEEE Power Energy Soc. Transmiss Distrib. Conf. Expo.*, Dallas, TX, USA, 2016, pp. 1–5.
[23] GAMS/SCENRED Documentation, 2016. [Online]. Available: http://www.gams.com/help/index.jsp
[24] ILOG CPLEX. ILOG CPLEX Homepage 2014. [Online]. Available: http://www.ilog.com
[25] M. Shahidehpour, H. Yamin, and Z. Li, *Market Operations in Electric Power Systems*, New York, NY, USA: IEEE, 2002.
[26] H. Wu, M. Shahidehpour, Z. Li, and W. Tian, "Chance-constrained day-ahead scheduling in stochastic power system operation," *IEEE Trans. Power Syst.*, vol. 29, no. 4, pp. 1583–1591, Jul. 2014.
[27] Q. Wang, C. B. Martinez-Anido, H. Wu, A. R. Florita, and B.-M. Hodge, "Quantifying the economic and grid reliability impacts of improved wind power forecasting," *IEEE Trans. Sustain. Energy*, vol. 7, no. 4, pp. 1525–1537, Oct. 2016.

Mingjian Cui (S'12–M'16) received the B.E. and Ph.D. degrees from Wuhan University, Wuhan, China, all in electrical engineering and automation, in 2010 and 2015, respectively.

He is currently a Research Associate and a Postdoctor at the University of Texas at Dallas, Richardson, TX, USA. From 2014 to 2015, he was also a Visiting Scholar in the Transmission and Grid Integration Group, National Renewable Energy Laboratory, Golden, CO, USA. His research interests include renewable energy forecasting, power system operation and control, unit commitment, economic dispatch, optimization modeling, electricity market, and data analytics.

Jie Zhang (M'13–SM'15) received the B.S. and M.S. degrees in mechanical engineering, in 2006 and 2008, respectively, both from Huazhong University of Science & Technology, Wuhan, China and the Ph.D. degree in mechanical engineering from Rensselaer Polytechnic Institute, Troy, NY, USA, in 2012.

He is currently an Assistant Professor in the Department of Mechanical Engineering, University of Texas at Dallas, Richardson, TX, USA. His research interests include multidisciplinary design optimization, complex engineered systems, big data analytics, wind energy, renewable integration, and energy systems modeling and simulation.

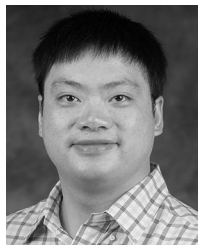

Hongyu Wu (SM'15) received the B.S. degree in energy and power engineering and the Ph.D. degree in systems engineering, both from Xi'an Jiaotong University, Xi'an, China, in 2003 and 2011, respectively. He is currently an Assistant Professor in the Department of Electrical and Computer Engineering, Kansas State University (K-State), Manhattan, KS, USA. From 2011 to 2014, he was a Postdoctoral Researcher in the Robert W. Galvin Center for Electricity Innovation, Illinois Institute of Technology in Chicago, Chicago, IL, USA. Before joining K-State, he worked as a Research Engineer in the Power Systems Engineering Center, National Renewable Energy Laboratory. His research interests include modeling and optimization of large-scale systems, power system operation and control, home energy management, and smart grid technologies.

Bri-Mathias Hodge (M'10) received the B.S. degree in chemical engineering from Carnegie Mellon University, Pittsburgh, PA, USA, in 2004, the M.S. degree from the Process Design and Systems Engineering Laboratory, Åbo Akademi, Turku, Finland, in 2005, and the Ph.D. degree in chemical engineering from Purdue University, West Lafayette, IN, USA, in 2010.

He is currently the Manager of the Power System Design and Studies Group, National Renewable Energy Laboratory, Golden, CO, USA. His current research interests include energy systems modeling, simulation, optimization, and wind power forecasting.